*Met. Mater. Int., Vol. 22, No. 1 (2016), pp. 101~107*
doi: 10.1007/s12540-016-5470-6

# Effects of Vanadium Content on the Microstructure and Dry Sand Abrasive Wear of a Eutectic Cr-Fe-C Hardfacing Alloy

**Hsuan-Han Lai, Chih-Chun Hsieh, Chi-Ming Lin, and Weite Wu***

Department of Materials Science and Engineering, National Chung Hsing University,
250 Kuo Kuang Road, Taichung 402, Taiwan, R.O.C

(received date: 1 September 2015 / accepted date: 10 November 2015)

In this study, the effects of vanadium on the morphology and wear behavior of a eutectic Cr-Fe-C hardfacing alloy were discussed. The alloys tested contained different amounts of vanadium, ranging from 0 to 2.39 wt%. A fibrous $V_4C_3$ was found when the alloy contained 0.93 wt% vanadium. The addition of vanadium was found to decrease the fraction of eutectic $M_{23}C_6$ and increase the width of the interspaces between the eutectic cells. The DTA results revealed that $V_4C_3$ formed just before the eutectic $\alpha+M_{23}C_6$ during solidification. The surface hardness was shown to increase with increasing vanadium content, which also caused the hardness deviation and wear loss to decrease; however, the addition of vanadium was not shown to affect the hardness of eutectic $\alpha+M_{23}C_6$. The $V_4C_3$ could be scratched off during the wear test due to the increase in the width of the interspaces between the eutectic cells; therefore, the alloys that contained 0.93 and 2.39 wt% vanadium exhibited similar wear loss results.

**Keywords:** eutectic carbide, welding, microstructure, wear, image analysis

## 1. INTRODUCTION

Abrasive wear occurs in many industrial processes. To resist abrasion, hardfacing alloys can be applied to work pieces to act as resistant coatings. Hardfacing can be applied using several techniques, such as plasma spraying, laser cladding, thermal spraying and welding processes [1]. Abrasion resistant materials consist of hard reinforcement phases, primarily carbides or borides, and a metal matrix. One of the most common hardfacing alloys is the chromium-carbide-reinforced alloy [1]. The Cr-Fe-C hardfacing alloys are widely used in mining and mineral processing industries due to the high fraction of carbide reinforcements. These alloys can be made of a martensite, austenite or ferrite matrix with $M_7C_3$ or $M_{23}C_6$ carbide as the reinforcement [1-5].

Additive elements such as niobium, titanium, molybdenum and vanadium can improve the wear resistance of Cr-Fe-C alloys [6-8]. These elements are strong carbide formers that help form secondary carbides in the hardfacing alloys [9]. The addition of vanadium reduces the primary carbide size in the hypereutectic alloy and increases its resistance to abrasion [7,10]. The Cr-Fe-C alloy is typically characterized by three different morphologies (hypoeutectic, eutectic and hypereutectic), depending on the carbon content present. The effect of vanadium on hypereutectic alloys has been described in detail in previous studies, while its effects in hypoeutectic and eutectic alloys still require additional examination. This study discussed the effect of vanadium on the microstructure and wear behaviors of a eutectic Cr-Fe-C hardfacing alloy.

*Corresponding author: wwu@dragon.nchu.edu.tw


## 2. EXPERIMENTAL PROCEDURES

The base metal substrates for the welding processes in the experiments of this study were prepared from S45C steel plates (0.48 wt% C, 0.2 wt% Si, 0.7 wt% Mn, 0.1 wt% Cr, and 98 wt% Fe) with dimensions of 50 mm × 50 mm × 20 mm. Before welding, the substrates were ground and cleaned with acetone. The fillers used were mixtures of pure chromium, carbo-chromium powder (20 wt% carbon) and carbo-vanadium powder (4 wt% carbon), which were mixed in a mechanical mixer; these compositions are listed in Table 1, and all fillers were designed to have a mass of 13 g. Compact fillers with dimensions of 30 mm × 25 mm × 3 mm were formed after the powders were prepared at a constant high pressure of 2200 psi (15.17 $N \cdot m^{-2}$).

Gas tungsten arc welding (GTAW) was performed with an oscillating traversing path. The welding torch used was installed on an automated system that carried the torch back and forth at a constant speed above the filler. The welding parameters included a welding voltage of 15 V, a welding current of 200 A, an argon flow rate of 15 $L \cdot min^{-1}$, a torch traveling speed

**Table 1.** Filler compositions

| Alloy | Element (wt%) | | | Powder (g) | | |
|---|---|---|---|---|---|---|
| | C | Cr | V | Cr-C | Cr | V-C |
| A | 4.0 | 96.0 | 0 | 2.6 | 10.4 | 0 |
| B | 4.0 | 95.0 | 1.0 | 2.57 | 10.29 | 0.14 |
| C | 4.0 | 94.0 | 2.0 | 2.55 | 10.18 | 0.24 |
| D | 4.0 | 92.0 | 4.0 | 2.492 | 9.968 | 0.54 |

of 20 mm·min$^{-1}$ and an oscillating speed of 250 mm·min$^{-1}$.

The chemical compositions of the clad alloys were analyzed with an electron probe microanalysis device (EPMA, JOEL JXA-8500F). The crystal structures were determined by X-ray diffraction (XRD, MXT III) with Cu Kα radiation (λ=1.54 Å) at 40 kV, 30 mA and a scanning range of 20-100° in a step-scan mode (0.02° per step). The recorded spectrum was matched against the data from the Joint Committee of Powder Diffraction Standards (JCPDS) to identify the crystal structures of each phase. The microstructure of the claddings was observed using an optical microscope (OM) and a field-emission scanning electron microscope (FE-SEM, JOEL JSM6700). The etchant was composed of 20 g of $NH_4F·HF$ and 0.5 g of $K_2S_2O_5$ in 100 mL of deionized water. Surface phase fractions were measured using an image analysis software (Image-Pro Plus, ver. 4.5.0). Ten pictures at 100 magnifications were taken for quantitative measurements. The phase transitions during the heating process in the alloy were determined by differential thermal analysis (DTA) under an argon atmosphere. The flow rate of argon was 4 L·min$^{-1}$, the heating rate was 10 °C·min$^{-1}$, and the highest temperature reached was 1500 °C. The surface hardness was determined using a Rockwell hardness tester (C scale) and a Vickers hardness tester with a 0.49 N (0.05 kg) load. Wear tests were performed in a dry-sand rubber-wheel testing machine based on ASTM G65-04 standards. Rounded quartz particles with mean diameters between 200 and 300 μm and hardness values of 1000-1100 HV were used. The sand flow rate was approximately 350 g·min$^{-1}$, and the chosen test load was 130 N (13.27 kg). The speed of the dry-sand rubber wheel was set to 200 rpm. After the wear test, the worn surface of a alloy was examined using a scanning electron microscope (JOEL JSM5400).

## 3. RESULTS AND DISCUSSION

### 3.1. Composition and phases

The elemental compositions of all of the alloys are listed in Table 2. The vanadium content was the primary difference between the four alloys and varied between 0 and 2.39 wt%. Chromium, iron and carbon were the primary components of the alloys, and their contents varied from 65.57 to 68.03 wt%, 26.29 to 28.23 wt%, and 3.22 to 3.39 wt%, respectively. Silicon, manganese and oxygen originated from the base metal and acted as impurities. Both chromium and vanadium were diluted with the base metal during welding.

**Table 2.** Chemical compositions of alloys (wt%)

| Alloy | Si | Fe | C | V | Mn | Cr | O |
|---|---|---|---|---|---|---|---|
| A | 0.08 | 26.25 | 3.22 | 0 | 0.38 | 66.43 | 1.56 |
| B | 0.06 | 26.23 | 3.31 | 0.54 | 0.51 | 68.03 | 1.23 |
| C | 0.09 | 28.23 | 3.39 | 0.93 | 0.45 | 65.57 | 1.24 |
| D | 0.08 | 25.29 | 3.38 | 2.39 | 0.43 | 66.53 | 1.26 |

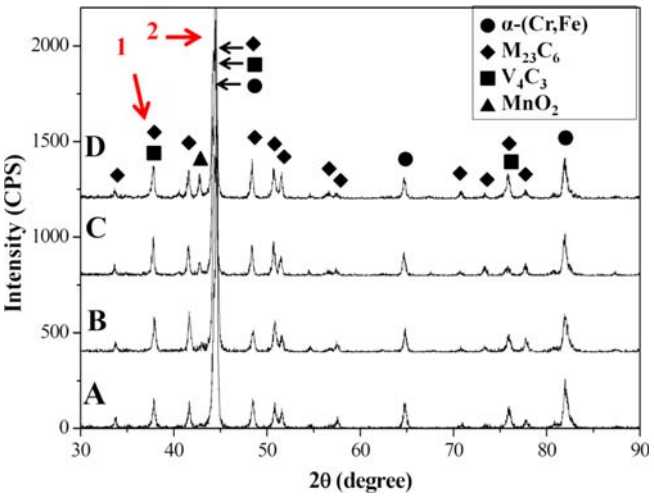


**Fig. 1.** Diffraction patterns of all alloys.

Figure 1 shows the diffraction results of the four alloys. The diffraction results show that all four alloys consisted of α phase (i.e., a solid solution of iron and chromium) and $M_{23}C_6$ carbides ("M" indicates metal elements). These are the two primary phases of a high-chromium Cr-Fe-C system. The vanadium carbide ($V_4C_3$) showed diffraction peaks that matched the diffraction pattern. The diffraction peaks of $V_4C_3$ could not be observed clearly because they overlapped with the peaks of $M_{23}C_6$; however, a change in the peak width could still indicate the existence of $V_4C_3$. The peak widths of the two marked peaks are shown in Table 3. As the vanadium content of the alloy increased from 0 to 2.39 wt%, the width of Peak 1 increased by 0.08°, and the width of Peak 2 increased by 0.1°. The appearance of the $V_4C_3$ peaks broadened the $M_{23}C_6$ peaks; there was also a diffraction peak of $MnO_2$ located at 42°. Because the fillers did not contain manganese, the source of the manganese observed in the results was likely the base metal.

**Table 3.** Peak widths of marked peaks in Fig. 1

| Alloy | Peak width (degree) | |
|---|---|---|
| | Peak 1 | Peak 2 |
| A | 0.281 | 0.434 |
| B | 0.334 | 0.513 |
| C | 0.336 | 0.529 |
| D | 0.361 | 0.539 |

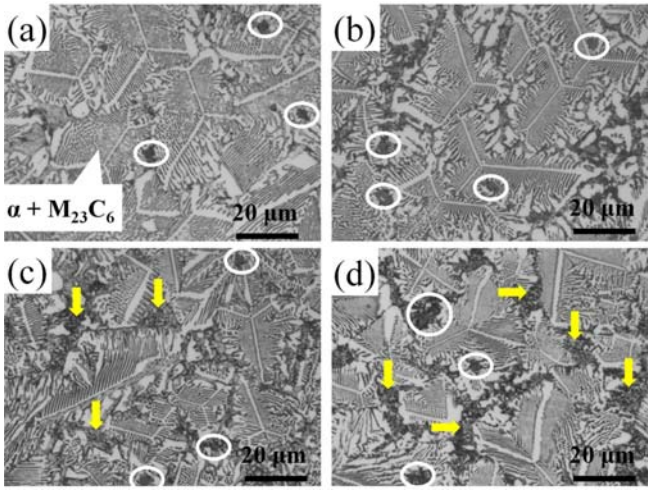


**Fig. 2.** OM images of (a) alloy A, (b) alloy B, (c) alloy C, and (d) alloy D.

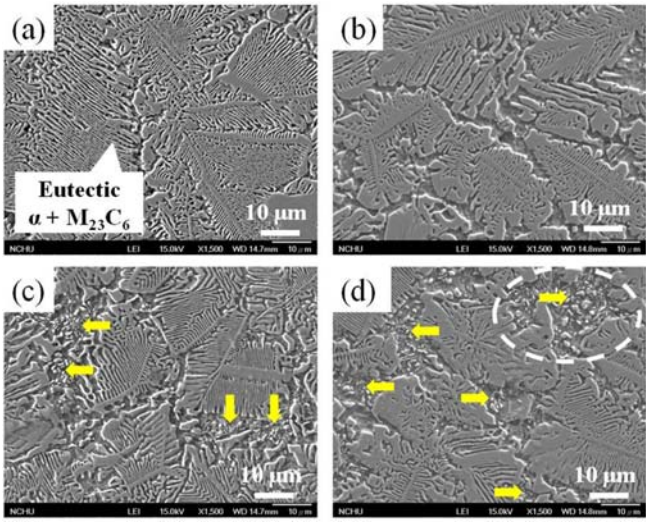


**Fig. 3.** SEM images of (a) alloy A, (b) alloy B, (c) alloy C, and (d) alloy D.

### 3.2. Microstructural evolution

The OM images of the clad alloys are shown in Fig. 2. All four alloys showed a eutectic structure that consisted of lamellar $M_{23}C_6$ carbide and an inter-lamellar α phase. It is shown that $M_{23}C_6$ lamellae were connected to a spine, and three spines linked to form a eutectic cell; this is the typical eutectic α+$M_{23}C_6$ structure that has been reported in the literature [11,12]. In alloy A, all eutectic cells remained near each other and had few interspaces between them. Additionally, it is shown that there were a few black particles (red circles) that were located within the interspaces. These particles are likely not particles of vanadium carbide because alloy A did not contain vanadium, as shown in Table 3; the particles might be $MnO_2$ inclusions because $MnO_2$ was found in the diffraction pattern. Alloy B contained eutectic cells and inclusion particles, as found in alloy A; however, it is shown that the interspaces between the eutectic cells in alloy B were broader and more apparent than those in alloy A. The eutectic cells could be distinguished from each other in alloy B because the interspaces were present. Because the vanadium content was the only difference between alloys A and B, the broadening of the interspaces must have resulted from the addition of the vanadium. In alloy C, the interspaces were more apparent than those in alloy B; there were also many small particles (yellow arrows) that were distributed in the interspaces between the eutectic cells. These small particles differed from the black particles in size and were only found in alloy C; these small particles were not found in alloy B. Alloy D exhibited a morphology similar to that of alloy C but contained significantly more small particles in its interspaces. Comparing the morphologies of the four alloys, it could be concluded that as the vanadium content increased, the interspaces between the eutectic cells increased and became more significant; also, small particles appeared and became more distributed in the interspaces when the vanadium content reached 0.93 wt%. Black particles were also found in the alloys whether vanadium was present or not.

Figure 3 shows the SEM images of the four alloys. Using the secondary image mode, the eutectic morphologies and the small particles are clearly shown; however, the black particles shown in Fig. 2 are not shown in Fig. 3. The eutectic cells in alloy A are shown to be near to their neighboring eutectic cells, as shown by the OM. The interspaces between the eutectic cells became wider in alloy B, and no particles were found in these interspaces. The small particles appeared in alloys C and D and were found to be distributed in the interspaces. A close view of the circled area of alloy D is shown in Fig. 4. The small particles exhibit a fibrous structure, and the EDS spectrum revealed that these fibers and globes contained vanadium and carbon; the fibers are thus likely $V_4C_3$, which was measured in the XRD pattern. It has been reported that the fibrous or small vanadium carbide particles origi-

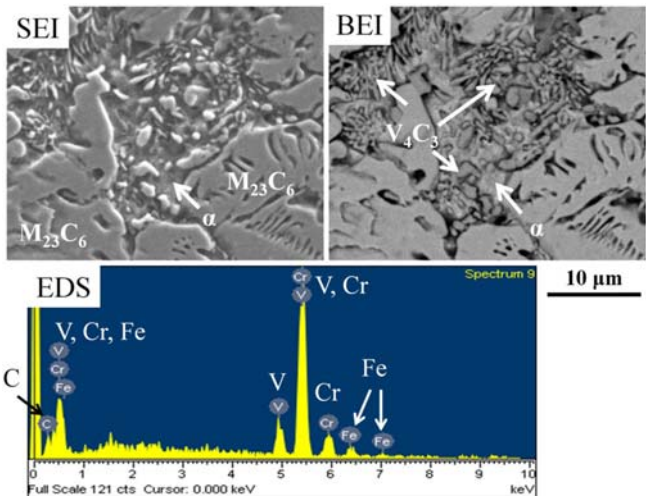


**Fig. 4.** SEM images and EDS spectrum of $V_4C_3$.

nated from a eutectic transformation [13-16]. In Adnane's report, the eutectic austenite+VCx with a fibrous structure solidifies just before the eutectic austenite+$M_7C_3$ structure; the two eutectic phases also have similar melting points, which are 1297 and 1284 °C, respectively [13]. In this study, the fibrous $V_4C_3$ might be a eutectic structure that solidified just before the α+$M_{23}C_6$ eutectics. To examine the phase transformation temperature of the alloys, a DTA was performed, and the two heating curves of alloy A and D are shown in Fig. 5. The melting point of alloy A was 1298.6 °C. Because alloy A was a fully eutectic α+$M_{23}C_6$ alloy, it had only one melting point, and there was only one endothermic peak on the curve. The melting point of alloy D was determined to be 1302.5°C; this should be the melting point of the eutectic α+$M_{23}C_6$. However, it is also shown that there were two endothermic peaks on the curve (blue arrows). Thus, there must be another melting reaction that had a higher melting point than 1302.5 °C, even though the temperature could not be determined from the curve shown. However, it could still be concluded that the $V_4C_3$ must have solidified as a eutectic structure of α+$V_4C_3$ before the formation of eutectic α+$M_{23}C_6$ during welding.

A peak indicating the presence of $MnO_2$ also appeared in the XRD results. The EDS results, as shown in Fig. 6, shows that the particles, which were larger than the $V_4C_3$ particles, were in fact $MnO_2$. Additionally, vanadium was found to have dissolved into the $MnO_2$ particles, as shown in the spectrum of alloy D. Compared to Fig. 2, it is shown that the $MnO_2$ particles were present in all of the alloys. Because the fillers did not contain vanadium, the base metal must be the source of this manganese. The microstructure of the base metal is also shown in Fig. 6. Particles also appeared in the base metal; however, the EDS results showed that these particles were composed of manganese sulfide, which is a common inclusion in steels. Manganese will typically interact with sulfur in molten iron during steel making and form manganese sulfide as an inclusion in the cast. The source of oxygen can be the weld metal, filler, flux or the air [17]. GTAW used Ar as a shielding gas to avoid oxygen in the air, but could not avert it from the weld metal and filler. In this study, the fillers were pieces of compact powders, so the air was trapped in the filler and acted as the source of oxygen. This manganese sulfide can also interact with oxygen to form oxides (i.e., slag) [18]. The addition of vanadium promotes the formation of $MnO_2$, and the vanadium tends to dissolve into the $MnO_2$ [19]. Therefore, the $MnO_2$ in alloy D contained vanadium, while that in alloy A did not.

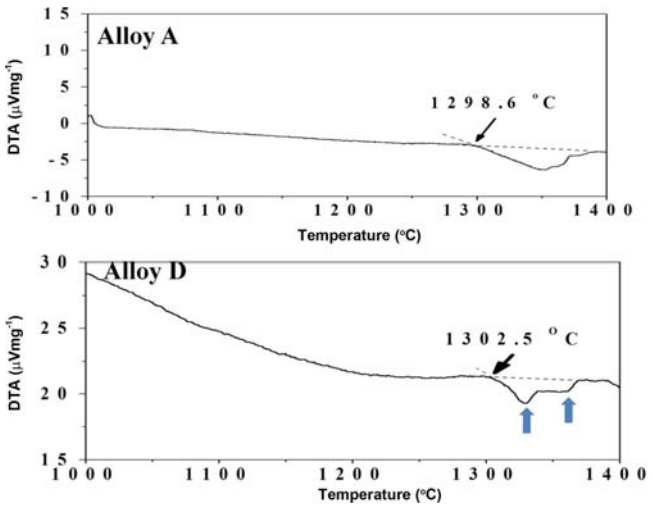


**Fig. 5.** DTA curves of alloy A and D.

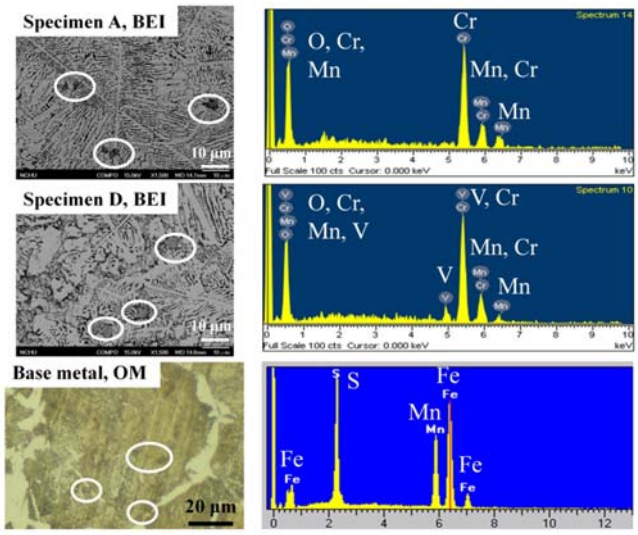


**Fig. 6.** $MnO_2$ particles in the alloys, and MnS in the base metal.

The phase fractions of all of the alloys are shown in Table 4. The $V_4C_3$ phase was not found in alloys A and B; thus, its fraction in these two alloys was not calculated. The $V_4C_3$ fraction was found to increase as the vanadium content increased in alloys C and D. The $M_{23}C_6$ fraction decreased from 60.67 to 51.84% as the vanadium content increased, while the total carbon content remained constant. In contrast with the $M_{23}C_6$ fraction, the amount of α increased from 38.05 to 42.95%. Vanadium has been considered to be a strong carbide former; it also has a higher affinity to combine with carbon than with chromium. As discussed earlier, the $V_4C_3$ solidified just before the $M_{23}C_6$. When the alloy solidified, vanadium adsorbed onto carbon to form carbides before chromium [9]; the resulting

**Table 4.** Fractions of all phases in each alloy

| Alloy | Phase fraction (%) | | | |
|---|---|---|---|---|
| | α | $M_{23}C_6$ | $V_4C_3$ | $MnO_2$ |
| A | 38.05 | 60.67 | - | 1.26 |
| B | 40.16 | 58.03 | - | 1.6 |
| C | 41.27 | 56.22 | 1.34 | 1.16 |
| D | 42.95 | 51.84 | 4.05 | 1.15 |

depletion of carbon in the liquid phase resulted in a lower amount of chromium carbides after the vanadium carbides formed. An increase in the vanadium content will thus push the eutectic composition to have a higher carbon content [7]; therefore, in a hypereutectic alloy, the amount of primary carbide decreases, while the amount of eutectic structure increases. The additional vanadium content will change the morphology of the material from a hypereutectic to a hypoeutectic structure. In this study, the amount of eutectic $M_{23}C_6$ decreased with the increase in vanadium content, while the amount of α phase increased. Although an alloy's composition does not represent the absolute eutectic composition, a completely eutectic structure can still form over a range of compositions near the eutectic composition [20]. Therefore, in this study, the four alloys exhibited a eutectic structure, even though the vanadium addition changed the eutectic composition. If the alloy contained additional vanadium content, a hypoeutectic structure, consisting of the primary α and eutectic $\alpha+M_{23}C_6$ phases, would replace the current eutectic morphology.

### 3.3. Surface hardness and wear behaviors

The hardness results, as shown in Fig. 7, show that the average hardness of the alloys without the addition of vanadium was approximately 46.1 HRC. With the addition of vanadium, the surface hardness increased to approximately 50.5 HRC when the vanadium content was 0.54 wt% and exhibited the highest hardness of 53.6 HRC when the alloy contained 2.39 wt% of vanadium. The surface hardness was thus shown to increase with the increase in vanadium content. Although the $V_4C_3$ in alloy B could not be observed with the microscope, the diffraction results showed that it was present. Besides, the hardness deviation decreased with the increase in vanadium content in alloy B, C and D. The addition of vanadium resulted in a reduction in the amount of $M_{23}C_6$ and an increase in the width of the eutectic structure interspaces. These interspaces became the weak point in alloy B, so the hardness deviation of alloy

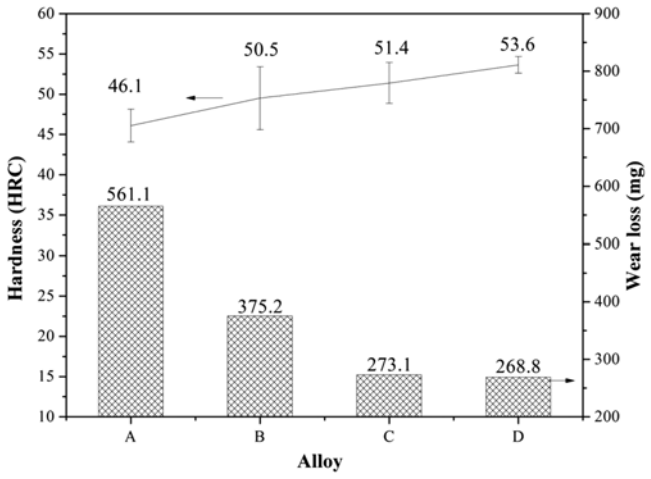


**Fig. 7.** Surface hardness and wear loss of each alloy.

**Table 5.** Vickers hardness of different structures

| Structure | $\alpha+M_{23}C_6$ (alloy A) | $\alpha+M_{23}C_6$ (alloy D) | $\alpha+V_4C_3$ (alloy D) |
|---|---|---|---|
| Hardness ($HV_{0.05}$) | 822.4±16.7 | 822.8±39.6 | 1020.6±15.9 |

B was greater than that for alloy A. As the vanadium content increased because $V_4C_3$ was distributed in the interspaces between the eutectic $M_{23}C_6$, the surface hardness of alloy D became more uniform than that of alloy B. Table 5 shows the Vickers hardness of the different structures in alloys A and D. The tested alloys did not include alloys B and C because $V_4C_3$ was not observed in alloy B and could not be precisely indented in alloy C; therefore, only alloys A and D were selected for testing. Without the addition of vanadium, the eutectic structure in alloy A exhibited a hardness of 822.4 HV. In alloy D, the structure of $\alpha+V_4C_3$ exhibited a hardness of 1020.6 HV, while the $\alpha+M_{23}C_6$ structure exhibited a hardness of 822.8 HV. The addition of vanadium did not affect the hardness of the $\alpha+M_{23}C_6$ structure. Therefore, the increase in the surface hardness was caused by the presence of $V_4C_3$. The wear losses were measured to be 565.1, 375.2, 273.1 and 268.8 for alloys A, B, C and D, respectively, and a lower wear loss was assumed to indicate a higher wear resistance. Additionally, higher vanadium content tended to result in a higher hardness and thus, a higher resistance to wear. Comparing alloys C and D, the difference in the wear loss between these two alloys was only 4.3 mg, even though alloy D had a higher vanadium content and a higher hardness than alloy C. The two alloys showed similar wear loss results, even though alloy D had twice the vanadium content of alloy C (0.93 and 2.39 wt% in alloys C and D, respectively). Vanadium carbide has been reported to resist abrasion [8,16]. It has also been reported that the wear resistance of a hardfacing alloy is determined by the carbide composition, size, shape and distribution [21]. Additionally, an increase in the carbide fraction can improve the wear resistance of an alloy [22]. In this study, the carbide fraction decreased as the vanadium content and the wear resistance increased. With the appearance of vanadium carbide, the wear resistance was found to improve, even though the total carbide fraction decreased. A schematic diagram was illustrated in Fig. 8. With the increase of vanadium content in clad alloys, $V_4C_3$ carbides could be observed in the interspaces of the eutectic $\alpha+M_{23}C_6$ cells, and the width of the interspaces also increased because of the decrease in the amount of $M_{23}C_6$ carbides. The formation of $V_4C_3$ carbides resulted in the increase in hardness and the decrease in wear loss because of the high hardness of the $V_4C_3$. It was also found that although additional vanadium content tended to result in a higher hardness, the increase in the wear resistance slowed after the vanadium content reached 0.93 wt%. Theoretically, higher vanadium contents could resist wear more effectively; however, the decrease in the wear loss was not significant after the vanadium

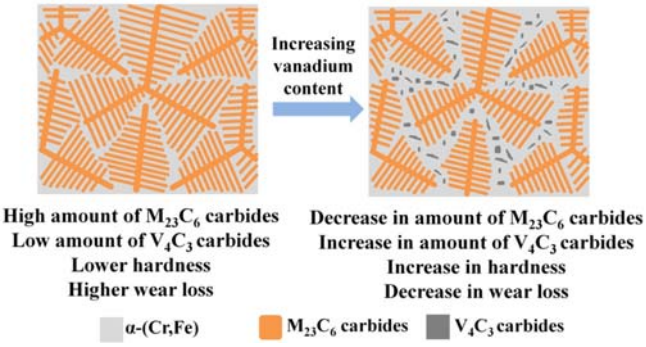


**Fig. 8.** Transition of eutectic Cr-Fe-C alloys with different vanadium contents.

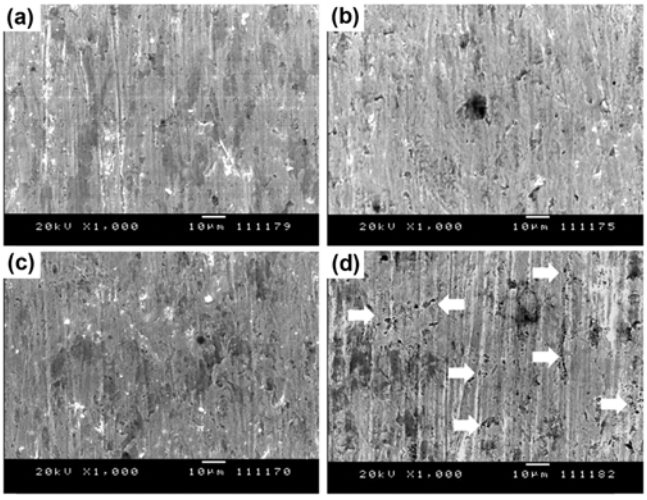


**Fig. 9.** Worn surfaces of (a) alloy A, (b) alloy B, (c) alloy C, and (d) alloy D.

content reached a certain value. Qi's reports that additional vanadium content tends to increase the presence of eutectic structure while the amount of primary carbide decreases; the alloy that contains the maximum vanadium content exhibited the lowest wear loss, but the value was near that which contains the second highest vanadium content [7]. In this study, all of the alloys exhibited a fully eutectic morphology; thus, the discussion of the primary carbide was not applicable. As a result, worn surfaces of the alloys were observed.

The worn surfaces are shown in Fig. 9. The results showed that all of the alloys exhibited discontinuous grooves on their surfaces (i.e. wear traces); these discontinuous grooves formed while the abrasives particles were interrupted during abrasion. In alloys A and B, few grooves were found and those found were deeper than the others found in other alloys; these grooves indicated that severe abrasion had taken place. In alloy C, no deep grooves were found, indicating that alloy C had a better abrasion resistance than alloys A or B; the wear loss result of alloy C also confirmed this finding. In alloy D, the worn surface exhibited grooves as well as many cavities (indicated by arrows). A detailed view of the cavities is shown

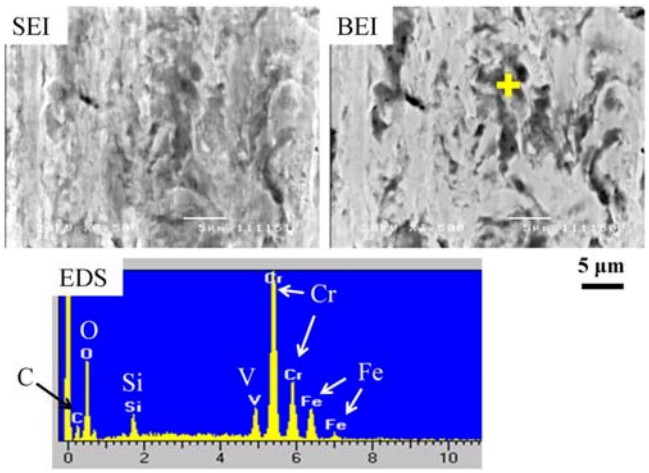


**Fig. 10.** Worn cavities of alloy D.

in Fig. 10. The EDS spectrum showed that the cavities contained vanadium; thus, the cavities must be the sites where $V_4C_3$ is located. Cavities can form when carbides are pulled from the surface of a material [23]. Thus, it could be concluded that the $V_4C_3$ was scratched off of the surface during the abrasion test. As shown in Fig. 3, $V_4C_3$ was distributed into the interspaces of the eutectic cells. Additionally, the width of the interspaces increased with the addition of vanadium because the $M_{23}C_6$ fraction decreased. The distance between the carbides determines whether abrasive particles can abrade the matrix and remove carbides [4]; if the distance between the carbides increased, abrasive particles could easily attack the interspaces. In this study, the addition of vanadium increased the interspaces between the eutectic cells. In alloy B, the interspaces were not sufficiently for the abrasive particles to attack the interspaces of the material; as a result, the worn surface was similar to that of alloy A. For alloys C and D, the interspaces contained $V_4C_3$, which acted as reinforcement, but the interspaces in alloy D were larger than those in alloy C. As illustrated in Fig. 11, the abrasive particles could attack and scratch the $V_4C_3$ off in alloy D, leaving cavities. Therefore, although there was a higher amount of $V_4C_3$ in alloy D, the reduction in the wear loss was similar to that of alloy C. Considering the cost of raw materials and wear performance, alloy C would thus be the best choice for practical applications of this material.

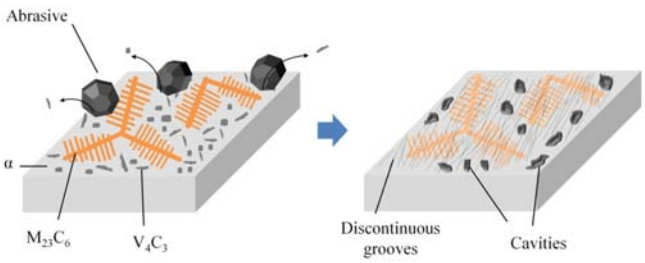


**Fig. 11.** The wear behavior of alloy D.

## 4. CONCLUSIONS

A eutectic Cr-Fe-C hardfacing alloy containing different amounts of vanadium was investigated in this study. The conclusions of this study are listed below:

(1) The addition of vanadium resulted in the formation of fibrous $V_4C_3$, which distributed into the interspaces between the eutectic $\alpha+M_{23}C_6$ cells.

(2) $V_4C_3$ solidified just before the eutectic $\alpha+M_{23}C_6$ during solidification.

(3) An increase in the vanadium content resulted in a decrease in the phase fraction of $M_{23}C_6$ present.

(4) The alloy's hardness was shown to increase as the vanadium content increased, while the hardness deviation and wear loss decreased.

(5) The $V_4C_3$ tended to be scratched off of the alloy's surface due to the increase in the interspaces between the eutectic cells.

## ACKNOWLEDGEMENT

The authors would like to acknowledge the financial support of the Ministry of Science and Technology under project NSC 102-2221-E-005-028-MY3.

## REFERENCES

1. P. F. Mendez, N. Barnes, K. Bell, S. D. Borle, S. S. Gajapathi, S. D. Guest, H. Izadi, A. K. Gol, and G. Wood, *J. Manuf. Process*. **16**, 4 (2014).
2. N. Yüksel and S. Şahin, *Mater. Des*. **58**, 491 (2014).
3. C. M. Lin, C. M. Chang, J. H. Chen, and W. Wu, *Mater. Sci. Eng*. **A 527**, 5038 (2010).
4. X. H. Tang, R. Chung, C. J. Pang, D. Y. Li, B. Hinckley, and K. Dolman, *Wear* **271**, 1426 (2011).
5. M. Shamanian, S. M. R. Mousavi Abarghouie, and S. R. Mousavi Pour, *Mater. Des.* **31**, 2760 (2010).
6. Q. Wang and X. Li, *Weld. J*. **89**, 133s (2010).
7. X. Qi, Z. Jia, Q. Yang, and Y. Yang, *Surf. Coat. Technol.* **205**, 5510 (2011).
8. J. Laurila, A. Milanti, J. Nurminen, M. Kallio, and P. Vuoristo, *Wear* **307**, 142 (2013).
9. M. Aksoy, O. Yilmaz, and M. H. Korkut, *Wear* **249**, 639 (2001).
10. X. Wang, F. Han, X. Liu, S. Qu, and Z. Zou, *Wear* **265**, 583 (2008).
11. C. M. Lin, C. M. Chang, J. H. Chen, C. C. Hsieh, and W. Wu, *Surf. Coat. Technol*. **205**, 2590 (2010).
12. C. Fan, M. C. Chen, C. M. Chang, and W. Wu, *Surf. Coat. Technol*. **201**, 908 (2006).
13. L. Adnane and R. Kesri, *J. Alloy. Compd*. **178**, 71 (1992).
14. J. D. B. De Mello and M. Durand-Charre, *Mater. Sci. Eng.* **67**, 109 (1984).
15. E. Fras, M. Kawalec, and H. F. Lopez., *Mater. Sci. Eng.* **A 524**, 193 (2009).
16. Y. Herrera, I. C. Grigorescu, J. Ramirez, C. D. Rauso, and M. H. Staia, *Surf. Coat. Technol*. **108-109**, 308 (1998).
17. S. Kuo, *Welding Metallurgy,* 2nd Edition, p.73, John Wiley & Sons, Inc., Hoboken, New Jersey (2003).
18. Y. K. Rao, *Stoichiometry and Thermodynamics of Metallurgical Processes*, p.778, Cambridge University Press, New York (1985).
19. D. Yang, *J. Power Sources* **228**, 89 (2013).
20. R. Elliott, *Encyclopedia of Materials: Science and Technology.* 2nd ed., pp.2816-2821, Elsevier Ltd. (2001).
21. M. F. Buchely, J. C. Gutierrez, L. M. León, and A. Toro, *Wear* **259**, 52 (2005).
22. J. J. Coronado, H. F. Caicedo, and A. L. Gómez, *Tribol. Int.* **42**, 745 (2009).
23. C. M. Chang, L. H. Chen, C. M. Lin, J. H. Chen, C. M. Fan, and W. Wu, *Surf. Coat. Technol.* **205**, 245 (2010).